Check for updates

Eulerian multiphase population balance model of atomizing, swirling flows

Narayana P. Rayapati*, Mahesh V. Panchagnula*,‡, John Peddieson*, John Short† and Steven Smith†

*Department of Mechanical Engr., Tennessee Tech University, Cookeville, TN 38505

‡Currently: Department of Applied Mechanics, Indian Institute of Technology Madras, Chennai, 600036 India

†Engine Components Business, Goodrich Corporation, West Des Moines, IA 50265

Received on August 26, 2010; Revised submission December 24, 2010; Accepted on February 04, 2011

ABSTRACT

An Eulerian/Eulerian multiphase flow model coupled with a population balance model is used as the basis for numerical simulation of atomization in swirling flows. The objective of this exercise is to develop a methodology capable of predicting the local point-wise drop size distribution in a spray, such as would be measured by the Phase Doppler Particle Analyzer (PDA). Model predictions are compared to experimental measurements of particle size distributions in an air-blast atomizer spray to demonstrate good qualitative and quantitative agreement. It is observed that the dependence of velocity on drop size inherent in a multiphase description of the drop cloud appears necessary to capture some features of the experimental data. Using this model, we demonstrate the relative contributions of secondary atomization and transport to the variation observed in the downstream spray drop size distribution.

1. INTRODUCTION

Atomization of a swirling liquid jet issuing into a surrounding gaseous medium plays an important role in many engineering processes. Atomization itself, involves a liquid jet or sheet being disintegrated by the kinetic energy of the liquid itself, or by exposure to a high velocity gas (typically air). Because of the random nature of the atomization process the resultant spray is usually characterized by a wide spectrum of drop sizes. In most combustion systems, reduction in mean drop size leads to higher evaporation rates and better mixing. Atomization is generally decomposed conceptually into primary and secondary components. Primary atomization occurs in the dense spray region near the nozzle where the liquid stream is broken up into shreds and ligaments. Secondary

*Corresponding author: mvp@iitm.ac.in

atomization occurs in the dilute spray region away from the nozzle where the shards and ligaments are further disintegrated into small droplets. The present paper is concerned with numerical prediction of atomization in swirling flows.

Atomizing flows lend themselves to a multiphase description in which a system consisting of one gas phase and a finite number of different drop phases (size classes) is analyzed. The accuracy of the description obviously increases with the number of size classes included. While an Eulerian description is almost always used for the continuous phase, both Lagrangian and Eulerian descriptions have been used for the discrete phases. The present discussion will be confined to models based on an Eulerian description of all phases (usually designated as Eulerian/Eulerian in the literature) because these are thought to be the most capable of modeling the large variations of particulate volume fractions observed in large scale industrial atomizer flows (dense to sparse spray regions). In models of this kind all phases are treated as continua (that is: continuous variables are used to represent the behaviors of all phases).

The literature on Eulerian/Eulerian modeling of particle/gas dispersions with multiple size classes is voluminous and will not be reviewed here (see Fox et al. [1] for a recent review) except to note that several approaches are possible. These will be discussed briefly below in order of increasing complexity. Mixture models (see, for instance Chen et al. [2]) are those in which the gas and all particle size classes are combined into a single equivalent fluid. Particulate mixture models (see, for instance, Chen et al. [2]) are created by combining all particulate size classes into a single equivalent fluid while allowing the gas to retain a separate identity. Multiple size group (MUSIG) models (see, for instance, Ghaniyari-Benis et al. [3]) group the size classes into a smaller number of equivalent fluids which, along with the gas, have separate identities. Full multiphase models (see, for instance, Kunz et al. [4]) allow all size classes and the gas to maintain separate identities. Classification overlap obviously exists. Thus, a MUSIG model with one equivalent fluid representing the particle cloud is a particulate mixture model while a MUSIG model with a number of equivalent fluids equal to the number of size classes is a full multiphase model. The present work employs a full multiphase model. The literature pertaining specifically to Eulerian/Eulerian multiphase spray modeling appears to be much more limited. Representative examples are the papers by Fox et al. [1], Vallet et al. [5], Sero-Guillaume and Rimbert [6], Jay et al. [7], Deux and Sommerfeld [8], Demoulin et al. [9], and Moukalled and Darwish [10]. All but the first (which employs a low volume fraction multiphase model) and last (which uses a multiple size group model) of these are based on mixture models. Thus there is no overlap between any of these references and the present work (which is based on a high volume fraction full multiphase model).

In the multiphase continuum mechanics description, both primary atomization and secondary atomization are treated as processes of mass transfer from larger to smaller size classes. Primary atomization begins with bulk liquid (typically in the form of a sheet or jet) and is characterized by high liquid volume fractions. Secondary atomization begins with the large drops or blobs resulting from the primary atomization and is characterized by low liquid volume fractions. The distinction between primary and secondary atomization is, of course, somewhat artificial because the transition from the

former to the latter is gradual rather than abrupt. One currently unresolved issue is that of developing mass transfer mechanisms that allow the sheet breakup associated with primary atomization to be mimicked by an equivalent process of atomization of large drops, as discussed by Apte et al. [11]. This and other issues make modeling of atomization mass transfer a field of research in itself, which is not the primary focus of the present work. In the present work a crude version of this mimicking is employed in which the sheet is replaced by an entering monodisperse high volume fraction drop cloud sized to the liquid injector dimensions. Thus, the present model does not capture the details of the primary breakup process but does capture the large liquid volume fraction aspect of primary atomization. In contrast, Eulerian/Lagrangian approaches (being inherently limited to low liquid volume fractions) are unable to capture any aspect of dense spray transport. The present model captures all details of the secondary breakup process. Since secondary atomization produces final drop sizes much smaller than those resulting from primary atomization, an accurate model of secondary atomization is vital to predicting the final drop size distribution.

It should be pointed out that, as far as mass transfer is concerned, there is no difference between a multiphase continuum mechanics description and a discrete population balance description. A recent review article by Le Moyne [12] points to the uniqueness and feasibility of the application of the population balance approach to modeling spray formation. More details of population balance mass transfer modeling can be found in the book by Ramkrishna [13].

The numerical difficulties associated with swirling single phase flows are well known. It is reasonable to assume that the large number of additional conservation equations associated with multiphase secondary atomization models might exacerbate these difficulties. The primary purpose of the present work is to investigate this issue using an existing Eulerian multiphase model. A secondary goal of this effort is to demonstrate a methodology for generating solutions based on this full multiphase formulation which could be used as standards of comparison for less computationally intensive mixture, particulate mixture, and multiple size group models consistent with the full multiphase formulation. Identifying the ranges of applicability of these models constitutes an important element in the characterization of the tradeoffs between accuracy and computational efficiency necessary for engineers to make rational choices of computational tools. The degree to which simplified models can capture the behavior predicted by the full multiphase model is of interest in itself even if that behavior is not fully in accord with experimental measurements.

2. GOVERNING EQUATIONS

In this section a standard single pressure Eulerian multiphase model of the type discussed by Kunz et al. [4] and employed in the FLUENT software (see ref [11] for more details on the specific implementation methodology) is described which can be employed to predict the behavior of a dispersion of several particle size classes in a gas. The gas will be designated as phase 0 and the particle size classes will be designated as phases 1, 2, 3 … M, thus creating an M + 1 phase transport problem with each phase having a separate velocity. In Eulerian multiphase models, balance laws for mass and

linear momentum are solved separately for each individual phase with the phases being allowed to interact through source terms. It is convenient to present the governing equations in the dimensionless form. Toward this end the respective dimensional mass, length, time and particle volume scales [M]: $\bar{\rho}_0\bar{R}^3$, [L]: $\bar{R}$ and [T] = $R/\bar{U}$ and [V]: $\bar{d}_1^3$ are selected where $\bar{R}$ is the nozzle outer radius, $\bar{\rho}_0$ is the gas density, $\bar{U}$ is the outer air stream axial velocity, and $\bar{d}_1$ is the largest size class particle diameter. Hereafter it be understood that all dependent and independent variables are dimensionless. The formulation to be presented below describes a Favre averaged description of turbulent flow, with all dependent variables being interpreted as mean values.

The respective balances of mass and linear momentum for the gas (i = 0) can be written as (see ref. [14])

$$\frac{\partial}{\partial t}(\alpha_0) + \nabla\cdot(\alpha_0\vec{v}_0) = 0 \tag{1}$$

$$\frac{\partial}{\partial t}(\alpha_0\vec{v}_0) + \nabla\cdot(\alpha_0\vec{v}_0\vec{v}_0) = -\alpha_0\nabla p + \nabla\cdot\bar{\bar{\tau}}_0 - \sum_{i=1}^{M}\frac{18\alpha_0\alpha_i f_i}{d_i^2 ReKn^2}(\vec{v}_0 - \vec{v}_i) \tag{2}$$

where α_0 is the gas volume fraction, $\vec{v}_0$ is the gas velocity, $Re = \bar{\rho}_0\bar{U}\bar{R}/\bar{\mu}_0$ is a Reynolds number ($\bar{\mu}_0$ being the continuous phase viscosity), p is a hydrodynamic pressure shared by all $M + 1$ phases, f_i is a drag function, and $Kn = \bar{d}_1/\bar{R}$ is a dimensionless number akin to a Knudsen number. The respective balances of mass and linear momentum for phase i can be written

$$\frac{\partial}{\partial t}(\alpha_i) + \nabla\cdot(\alpha_i\vec{v}_i) = -\Gamma_i\alpha_i + \sum_{j=1}^{(i-1)} n_{ij}x_i\Gamma_j\frac{\alpha_j}{x_j} \tag{3}$$

$$\begin{aligned}&\rho_i\left[\frac{\partial}{\partial t}(\alpha_i\vec{v}_i) + \nabla\cdot(\alpha_i\vec{v}_i\vec{v}_i)\right]\\ &= -\alpha_i\nabla p + \nabla\cdot\bar{\bar{\tau}}_i + \frac{18\alpha_0\alpha_i f_i}{d_i^2 ReKn^2}(\vec{v}_0 - \vec{v}_i) + \rho_i\left[-\Gamma_i\alpha_i\vec{v}_i + \sum_{j=1}^{(i-1)} n_{ij}x_i\Gamma_j\frac{\alpha_j}{x_j}\vec{v}_j\right]\end{aligned} \tag{4}$$

where α_i is the size class volume fraction, $\vec{v}_i$ is the size class velocity, $\rho_i = \bar{\rho}_i/\bar{\rho}_0$ is a density ratio, Γ_j is the atomization frequency of particles of volume x_j, and n_{ij} is the number fraction of particles of volume x_i formed from atomization of a particle of volume x_j. The combination $18\alpha_0\alpha_i f_i/d_i^2 ReKn^2$ plays the role of a dimensionless momentum exchange coefficient. The last term on the right hand side of equation (2) represents the drag applied to the gas by all size classes, the first term on the right hand side of equation (3) represents the rate of size class i mass loss to smaller size classes due to atomization, the last term on the right hand side of equation (3) represents the rate of size class i mass gain from larger size classes due to atomization, the third term on the right hand side of equation (4) represents the drag applied to size class i by the

gas, and the fourth and fifth terms on the right hand side of equation (4) represent the rates of linear momentum transfer to size class i associated with the afore mentioned mass gain and loss rates. In equations (2) and (4) the Newtonian stress tensor representation

$$\bar{\bar{\tau}}_i = \frac{\alpha_i \mu_i}{Re}\left[\left(\nabla \vec{v}_i + \nabla \vec{v}_i^{\,T}\right) - \frac{2}{3}\nabla \cdot \vec{v}_i \bar{\bar{I}}\right] \tag{5}$$

is used for all phases. Here $\mu_i = \bar{\mu}_i/\bar{\mu}_0$ is a viscosity ratio and $\bar{\bar{I}}$ is the unit tensor.

Turbulence is modeled by treating μ_i as an effective viscosity containing a turbulent component. A mixture k-ε model was used to characterize turbulent transport. This model is similar to the standard k-ε model except that mixture properties are used in the turbulence transport equations. The corresponding dimensionless transport equations for k and ε are given by

$$\frac{\partial}{\partial t}(\rho k) + \nabla \cdot (\rho k \vec{v}) = \nabla \cdot \left[\left(\mu + \frac{\mu_t}{\sigma_k}\right)\nabla k\right] + G_k - \rho\varepsilon \tag{6}$$

$$\frac{\partial}{\partial t}(\rho \varepsilon) + \nabla \cdot (\rho \varepsilon \vec{v}) = \nabla \cdot \left[\left(\mu + \frac{\mu_t}{\sigma_\varepsilon}\right)\nabla \varepsilon\right] + C_{1\varepsilon}\frac{\varepsilon}{k}(G_k) - C_{2\varepsilon}\rho\frac{\varepsilon^2}{k} \tag{7}$$

where

$$\rho = \sum_{i=0}^{M} \alpha_i \rho_i, \tag{8}$$

$$\mu = \sum_{i=0}^{M} \alpha_i \mu_i, \tag{9}$$

$$\vec{v} = \frac{\sum_{i=0}^{M} \alpha_i \rho_i \vec{v}_i}{\rho}, \tag{10}$$

G_k represents the generation of turbulence kinetic energy due to the mean velocity gradients, and $\bar{\mu}_t$ is the dimensionless turbulent viscosity. Values of the model constants σ_k, σ_ε, $C_{1\varepsilon}$, $C_{2\varepsilon}$ and details of G_k can be found in Launder and Spalding [15]. The relatively simple turbulence model described above was employed in order to focus attention on the potential for numerical difficulties associated with the large number of additional balance laws associated with a full multiphase approach to the simulation of atomizing swirling flows. It should be pointed out that this turbulence model does not allow the turbulence properties to be explicitly affected by the presence of the drops. However, computations performed with the so called dispersed k-ε model (which does

so allow) did not reveal any significant differences in predictions. For this reason, the mixture k-ε model was employed to produce the results to be reported subsequently.

The laminar contributions to the size class viscosity coefficients can be used for a number of purposes, such as the representation of same phase drop/drop interactions at large volume fractions. This is an evolving area of research in its own right and was thought to be beyond the scope of the current investigation. For this reason, values of the particulate laminar viscosity coefficients were employed that were of the same order of magnitude as the corresponding values of the gas viscosity coefficient. A limited parametric study indicated that predictions of the type described herein were insensitive to the exact values over two orders of magnitude (since the turbulent contributions always dominated).

The Schiller and Naumann [16] drag function

$$f_i = \begin{cases} 1 + 0.15 Re_p^{0.687} & \text{for } Re_p \le 1000 \\ \dfrac{0.44 Re_p}{24} & \text{for } Re_p > 1000 \end{cases} \tag{11}$$

thought to be appropriate for gas/liquid drop dispersions, was employed where

$$Re_p = \frac{\bar{\rho}_0 \left| \vec{\bar{v}}_0 - \vec{\bar{v}}_i \right| \bar{d}_i}{\bar{\mu}_0} = ReKn \left| \vec{v}_0 - \vec{v}_i \right| d_i \tag{12}$$

is a Reynolds number based on the velocity of the ith size class relative to the gas and the ith size class diameter d_i. The factor Kn in equation (12) has the effect of creating a change of scales from microscopic (drop-based) to macroscopic.

In order to demonstrate industrial applicability, FLUENT was used as the CFD engine to solve the set of governing equations described in this section (presented herein in the dimensionless form). However, the implementation of the terms associated with atomization mass transfer appearing in equations (3) and (4) required special attention in the context of the full multiphase model. This (and calculation of the associated coefficients, to be discussed later) was handled using the User Defined Function (UDF) capability to delineate the source terms in the mass and momentum equations. It was found necessary to use an unsteady solver to ensure numerical convergence. Even though the existence of a steady solution should be independent of whether the steady or unsteady solver is used, apparently differences in solution order exist which tend to favor the unsteady solver in this case. In addition, the time step often had to be adjusted down during the initial stages of the simulation to ensure numerical stability. Since a second order implicit discretization scheme was used, this does not appear to be a straight forward numerical stability issue such as that associated with explicit methods. It is more likely to be a convergence issue associated with atomization related stiffness during the early part of the computation. The numerical procedure outlined in Escue and Cui [17] for obtaining convergence in swirling flow fields was adapted to this multiphase flow situation.

Part of the numerical recipe mentioned above is the suggestion that the RNG k-ε model be used in place of the standard k-ε model when swirl becomes significant. Calculations were, therefore, performed with both versions of the mixture model. Since these did not reveal any significant differences in predictions, the standard k-ε mixture model was used to produce the results to be presented herein. Of course, no scalar turbulence model can be expected to fully characterize the turbulent anisotropy associated with swirling flows. Full Reynolds stress models are much more suited to this task. As stated earlier, the selection of a relatively simple turbulence model was motivated by a desire to focus on the potential numerical difficulties associated with the large number of balance laws associated with the full multiphase approach.

It is well known that Eulerian/Eulerian multiphase modeling is not a completely settled area and that many different forms of the basic balance laws have been proposed in the literature. Three examples are cited in this paragraph. First, the above described formulation assumes that all phases share a common hydrodynamic pressure. This assumption has been repeatedly questioned and many alternatives have been proposed. Second, the Favre averaging process does not produce turbulent diffusion terms in the mass balance equations (1) and (3). Instead, turbulent diffusion must be handled by including turbulent diffusion forces (proportional to volume fraction gradients) in the linear momentum balance equations (2) and (4) (see for instance, Lopez de Bertonado and Saif [18], Lopez de Bertonado [19] or Lopez de Bertonado et al. [20]). Such implementation could be handled by a UDF, but putting terms containing gradients in a source term has the potential to create numerical problems by changing the effective mathematical character of the equations. It was decided, therefore, to omit turbulent diffusion at this time. Third, the above described formulation assumes that the only interactions between the gas and the particulate phases are due to steady state drag. Many other contributions to the interphase forces are, of course, possible. It is not the purpose of the present work to make contributions to the resolution of these, or other (see, for instance, You et al. [21]) unresolved issues, but rather to investigate the feasibility of applying an existing multiphase model to the computation of swirling atomizing flows. Because of the large number of existing uncertainties in Eulerian/Eulerian multiphase flow modeling, it can be quite difficult to assign a disagreement between predictions and measurements to a unique cause. This issue will be discussed further below.

3. RESULTS AND DISCUSSION

In this section, numerical predictions are discussed for the case of an atomizing axisymmetric swirling jet. These results are compared with experimental data obtained from a swirling axisymmetric free jet spraying a calibration fluid MIL-PRF-7024 type 2 using a Phase Doppler Particle Analyzer (PDPA). Phase Doppler Anemometry (PDA) is a technique widely employed to experimentally characterize particulate flows in terms of velocity and particle size distributions. The nozzle was mounted on a traverse system and a full radial scan was performed in order to obtain PDA data at regularly spaced radial locations. Similar scans were performed at three axial locations at each condition. The data was post-processed to obtain the drop size *pdf*.

The performance of PDA in dense particulate systems is poor and subject to significant error. Recently, Qiu et al. [22] have proposed modifications to PDA to improve the measurement accuracy in dense sprays. In addition, Koh and Yoon [23] used an optical line patternator to measure particle size distribution in dense sprays. The main deficiency of the current state of the art in experimental diagnostics of particulate systems is that they are unable to explicitly conserve mass as discussed by Widmann et al. [24]. This has to be borne in mind while comparing volume flux measurements to numerical predictions. However, particle size is relatively more accurate and hence would form a reasonable set of measurements to evaluate numerical predictions.

One method of obtaining the atomization mass transfer characterizations mentioned above is to discretize a continuous population balance model. Such models involve a continuous distribution kernel, $\beta(x_i, x_j)$ describing the number probability distribution function of daughter particles x_i produced by a single breakage event of a parent particle x_j. A breakage frequency Γ_i describing the rate at which particles break up per unit time is also postulated. These two elements provide a complete description of the birth and death events associated with each member of the continuous particle size distribution and can, therefore, be used as the basis for a discretization. This can be done in various ways, with the methodology reported by Kumar and Ramkrishna [25] being representative and producing the distribution coefficients

$$n_{ij} = \int_{x_i}^{x_{i+1}} \frac{(x_{i+1} - V)}{(x_{i+1} - x_i)} \beta(V, x_k) dV + \int_{x_{i-1}}^{x_i} \frac{(x_{i-1} - V)}{(x_{i-1} - x_i)} \beta(V, x_k) dV \tag{13}$$

This equation provides for a way of converting a continuous *pdf* $\beta(V, x_k)$ to a set of discrete co-efficients n_{ij}. The only macroscopic constraint on the choice of n_{ij} arises from the conservation of mass during a single breakage event

$$\sum_{i=j}^{M} n_{ij} \frac{x_i}{x_j} = 1 \tag{14}$$

and is identically satisfied by equation (13). In addition, equation (13) allows the possibility of producing distribution coefficients consistent with Kolmogorov's hypothesis (see, for instance, Gorokhovski and Saveiliev [26] or Apte et al. [11]) that breakups of all sized particles produce the same number of particles.

For all the results discussed in this paper, the n_{ij} values are calculated using equation (13) and the breakage kernel

$$\beta(x_i, x_j) = \frac{2}{x_j} \tag{15}$$

Equation (15) is a binary equal fragments kernel which implies (see [25]) that two drops are produced by the breakups of all sized drops (consistent with Kolmogorov's hypothesis). It was observed that the Sauter Mean Diameter results are relatively

insensitive to the specific choice of this kernel (see ref. [27] for more details). In addition, the breakage frequency was calculated from

$$\Gamma_i = \Gamma_0 \left| \vec{v}_0 - \vec{v}_i \right| f_i \tag{16}$$

where

$$\Gamma_0 = \frac{\bar{\Gamma}_0 \bar{\mu}_0 \bar{R}}{\bar{\sigma}} \tag{17}$$

is a dimensionless breakage frequency number involving the surface tension $\bar{\sigma}$. Equation (17) represents qualitatively a balance between destructive drag and restorative surface tension forces acting on a single drop. The value of $\bar{\Gamma}_0$ was determined from matching model predictions to one set of experimental PDA data and used for all the results presented herein. It can be seen that the breakage frequency decreases with decreasing particle size (with the frequency of the smallest size class being equated to zero). It also decreases with decreasing relative motion, which causes atomization to cease at a sufficient distance from the nozzle. The form of the breakage kernel in equation (15) was varied and simulations performed. From these simulations, it was observed that the specific form of the kernel chosen here has little effect on the qualitative trends (for example, the local radial variation of Sauter Mean Diameter (d_{32})) presented in this paper.

Lefevbre [28] classifies liquid jet or sheet atomization as either classical or prompt. Equations (16) and (17) can be thought of as representing a simplified description of the latter. The idealized model employed herein was selected purposely to focus attention on the multiphase computational aspects of the problem. Nevertheless, as will be seen subsequently, this model is able to predict many qualitative features of the experimental data.

For the special case of an idealized plug flow atomizer the equations of the present model reduce to a version of those associated with Reid's [29] batch grinding problem, for which he presented analytical solution. Before proceeding with numerical simulations of swirling atomizing flows, numerical solutions were obtained to the plug flow atomizer problem and compared to this analytical solution, with good agreement being observed [30]. This lent confidence to the numerical results to be presented subsequently.

Figure 1 shows the computational domain and the mesh used. Swirling air (no particles) is injected through inlets A and C, while a monodisperse distribution of the largest size class (no air) is injected through the inlet B. A structured grid using quadrilateral elements was generated in the fluid domain. As can be observed from this figure, care has been taken to sufficiently resolve the region where high gradients are expected.

For all the results presented in this section r and z represent the radial and axial positions respectively. The axial particulate phase volume flux (q_z'') is given by

$$q_z'' = \sum_{i=1}^{M} q_{i,z}'' \tag{18}$$

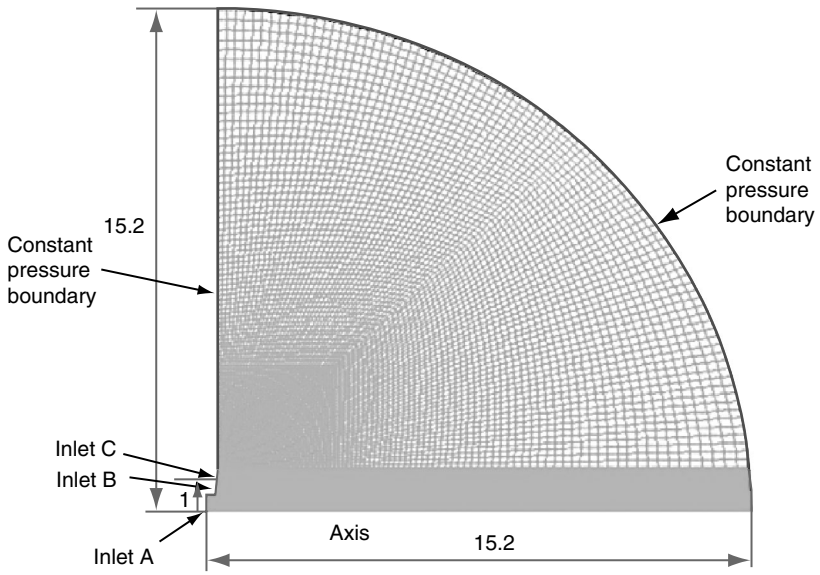

Figure 1: Computational domain with boundary conditions (coarse mesh with ~15 K cells shown here for clarity).

where $q''_{i,z}$ is the particle axial volume flux for the ith size class given by

$$q''_{i,z} = \alpha_i(\vec{e}_z.\vec{v}_i) \tag{19}$$

The results herein are presented in three forms. The first set of plots depicts the spray profile by indicating the region within the computational domain wherein q''_z is at least 4.5×10^{-3}. This plot is helpful in observing the macroscopic spray shape. The second set of plots depicts variation of the Sauter Mean Diameter (d_{32}) versus radial position (r) at various axial positions. The Sauter Mean Diameter, d_{32} is calculated using

$$d_{32} = \frac{\sum_{j=1}^{M} \alpha_j}{\sum_{j=1}^{M} \alpha_j / x_j^{1/3}} \tag{20}$$

The third set of plots present a comparison of the predicted particle size distribution at a few selected points with experimental measurements. The plots depict the number probability distribution function (*pdf*) versus particle size. The *pdf* can be calculated from the CFD simulations by knowing the values of α_i. The *pdf* for the ith particle size class is calculated as

$$pdf(i) = K \frac{2\left(\alpha_i / x_i\right)}{(d_{i-1} - d_{i+1})} \tag{21}$$

K is calculated from the normalization constraint that requires

$$\sum_{i=1}^{M} pdf(i)\frac{(d_{i-1}-d_{i+1})}{2}=1 \tag{22}$$

It must be mentioned that the probability data from the numerical simulations are known only at the particle size values associated with the discrete phases. However, the probability density function is a continuous function of particle size. While the $pdf(i)$ values calculated from equation (21) are indicated by markers on these graphs, the line connecting these markers is suggestive of the continuous probability density function.

The simulations to be discussed were run with ten size classes (M = 10). This decision was arrived at after a systematic study of the sensitivity of predictions to the value of M. It was observed that for M ≥ 10, the SMD results were independent of M [27]. Liquid injection through the inlet is comprised entirely of the largest size class phase (i = 1), taken (based on the experimental data) to be 250 μm herein. This value of drop size can be construed as being the result of the annular sheet breakup due to primary instability. Simulations were carried out for the two sets of inlet velocities, termed high flow and low flow, presented in Table 1. These are based on the exit conditions from single phase in nozzle simulations (at the same mass flow rate conditions as in the experiments) performed by the present authors and were not further

Table 1. Dimensionless inlet velocity conditions (the ratio of outer air axial velocity in high flow condition to that in the low flow condition is 2.484).

Normalized velocity components	High flow condition	Low flow condition
Inlet A		
Axial	1.3056	1.754
Radial	0.0129	0.0335
Swirl	–0.857	–1.4
Turbulent kinetic energy	0.00715	0.0408
Turbulent dissipation rate	0.03762	0.3069
Inlet B		
Axial	0.066	0.0408
Radial	0.01176	0.0094
Swirl	–0.0916	–0.054
Inlet C		
Axial	1	1
Radial	–0.5032	–0.529
Swirl	–1.2014	–0.9427
Turbulent kinetic energy	0.00835	0.0505
Turbulent dissipation rate	0.02997	0.8745
Re	5248	2122

adjusted to fit experimental observations. The values $Kn = 0.095$, $\mu_i = 0.5588$, $\rho_i = 619.9$, and $\Gamma_0 = 0.022$ were used to generate all the results to be discussed subsequently and, together with Table 1, completely characterize each simulation. All simulations were performed on Dell workstations with eight processors cores working in parallel. A typical simulation took about eight days of run time.

3.1. High flow condition simulation results

A grid independence study was performed, by gradually refining an initially coarse mesh. Figure 2 is a plot of q_z'' versus r at $z = 4.82$ for grids involving approximately 15000, 40000, 160000 and 600000 cells. Also shown in figure 2 is a plot of normalized d_{32} versus r at $z = 9.64$. As can be observed, the SMD predictions are grid independent for a domain consisting of at least 160000 cells. However, it was observed that volume flux predictions required one further mesh refinement beyond the 600000 cells to achieve complete grid independence. Because of the computer capability available, all the results presented herein are obtained on a mesh with at least 160000 cells. It is felt that this was sufficient to demonstrate the capabilities of the full multiphase approach. A typical simulation on this mesh took approximately 7 days running in parallel on eight 2.2 GHz cores.

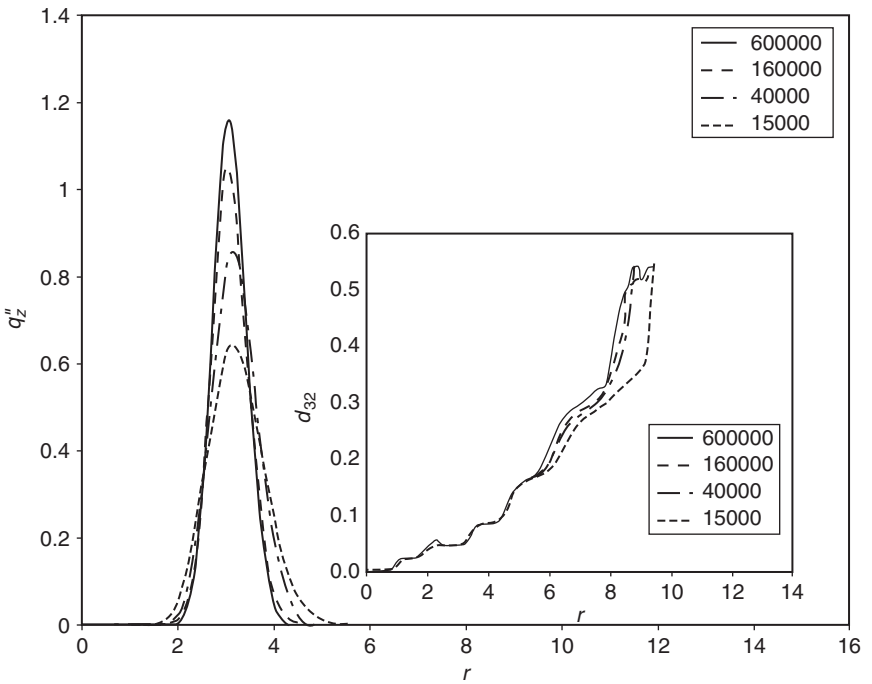

Figure 2: Radial profile of normalized volume flux at z = 4.82 for varying grid sizes. The inset figure shows radial profiles of the Sauter Mean Diameter at z = 9.64 obtained on the same grids.

Figure 3 is a plot of the spray profile obtained from the high flow simulation. Also shown in this figure are the air velocity vectors colored by the velocity magnitude. As expected for a swirling jet, the particles are all located in an annular region, indicating a hollow cone behavior.

Figure 4 reports radial profiles of normalized SMD obtained from the high flow numerical calculations at the three axial locations z = 3.61, 4.82 and 9.64; together with the corresponding PDA data. It can be observed that the numerical predictions and experimental measurements exhibit the same qualitative trends at all three axial locations. In particular, the slopes of the predicted and observed radial profiles of d_{32} seem to match quite well. There is, however, a consistent quantitative numerical under prediction of the absolute values of d_{32}. This appears to be mainly due to the predicted SMD being nearly zero for small values of r. Considering that this model has no experimentally determined input parameters, the level agreement is very encouraging.

Figures 5a, b and c present number *pdf* versus normalized drop size from the high flow simulations. These plots are generated at points A, B, and C in figure 3 where the drop volume flux was high and experimental data was available. It can be observed that predicted and measured drop size distributions are in reasonable agreement.

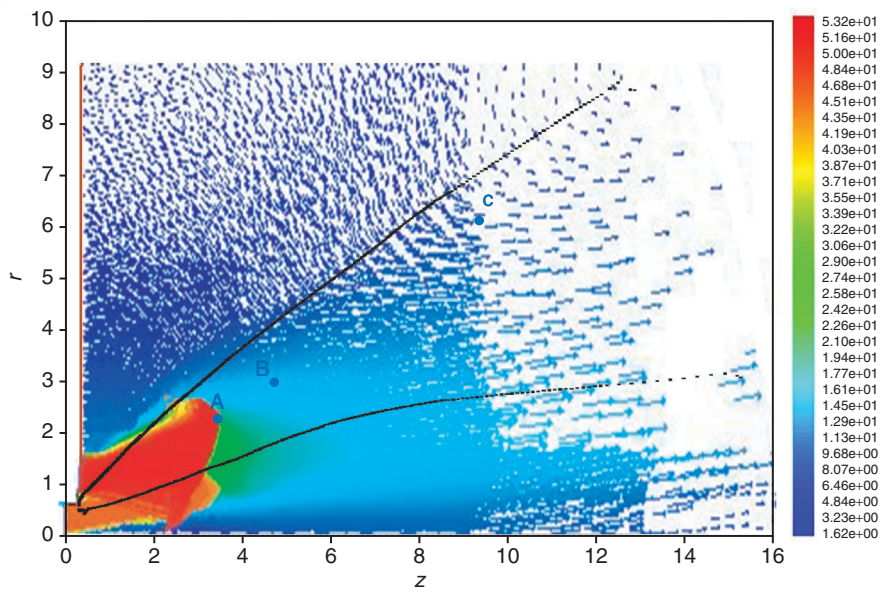

Figure 3: Spray profile (black dotted line) obtained from high mass flow rate case simulation overlaid on a velocity vector plot colored by velocity magnitude (red and blue indicate highest and lowest velocities respectively).

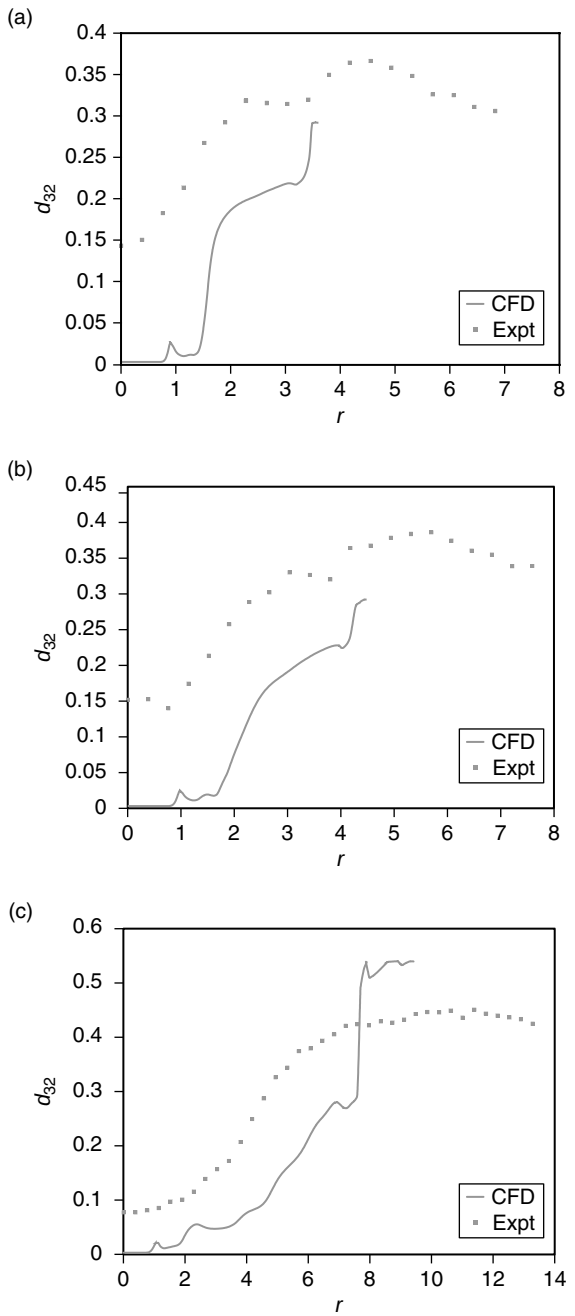

Figure 4: Radial profiles of normalized SMD obtained from the high flow condition simulation at axial locations of (a) 3.61, (b) 4.82 and (c) 9.84.

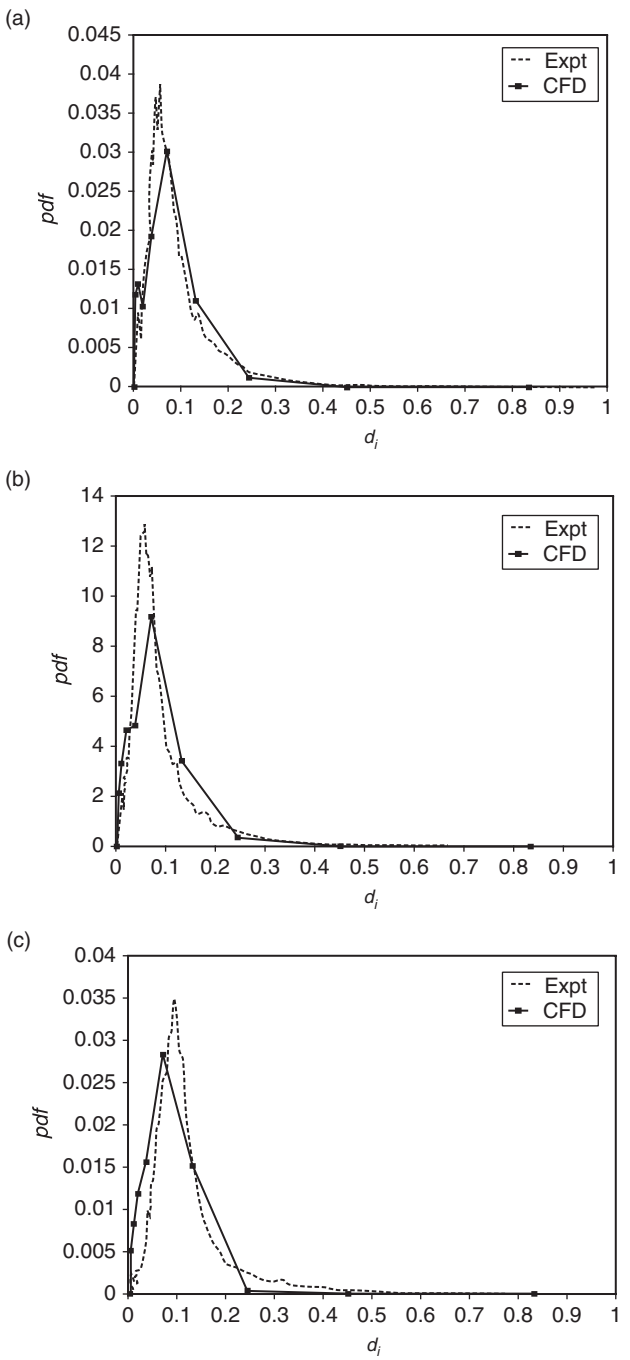

Figure 5: (a) Particle size distribution *pdf* at z = 3.61, r = 2.26 and at the high flow condition. (b) Particle size distribution *pdf* at z = 4.82, r = 3.01 and at the high flow condition. (c) Particle size distribution *pdf* at z = 9.64, r = 6.18 and at the high flow condition.

In comparing the *pdf* presented in figure 5 with the corresponding data points in figure 3, it can be observed that while the experimental and computed particle size *pdf* are in reasonable agreement, the Sauter mean diameter is under-predicted by the CFD model. This is because the Sauter mean diameter is skewed by the larger particles in the distribution. Again, there are many plausible explanations, but one that should be investigated is that of assigned size class distribution. The simulations reported herein are based on the size classes being arranged in a geometric progression similar to the work of Kumar and Ramkrishna [25].

Figure 6 is a plot of the radial distribution of the normalized total axial drop volume flux at the axial location z = 4.82, together with the corresponding experimental measurements. It can be seen that the drop volume is mostly concentrated in an annular region. It can be further observed that the measured radial spread is significantly higher than the corresponding numerical prediction. Complete agreement is not expected, however, because it is well known that PDA volume flux measurements considerably over estimate particulate volume flux. Using this data, for example, radially integrating the axial liquid volume flux yields a total liquid volume flow rate approximately 40% higher than the measured injector liquid volume flow rate. It is also possible that particle dispersion is under estimated by the model, which uses a single hydrodynamic pressure shared by all phases.

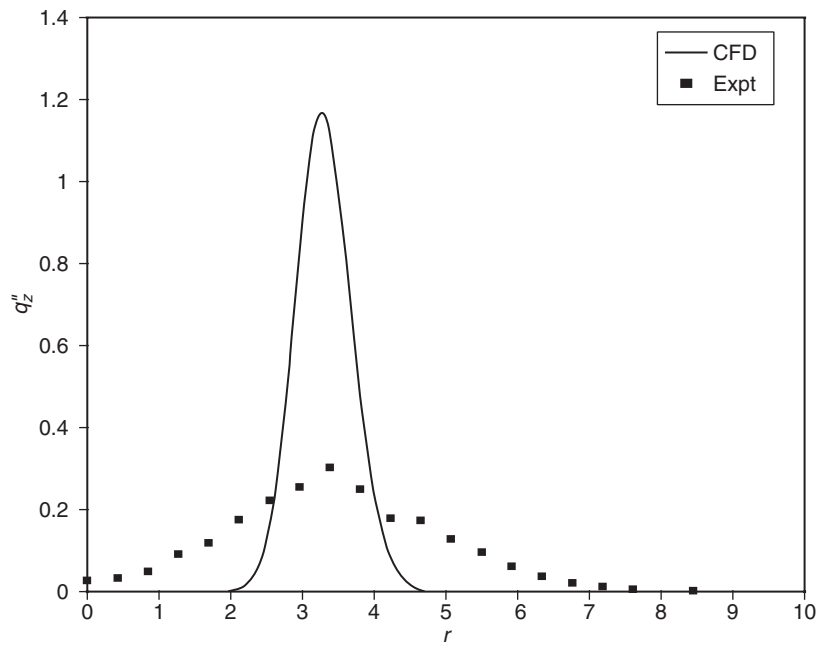

Figure 6: Radial profile of normalized volume flux at z = 4.82 for the high flow condition simulation.

3.2. Low flow condition simulation results

Figure 7 is a plot of the spray profile obtained from the low flow simulation. The qualitative behavior of the spray is observed to be same as that of high flow simulation, with the spray angle being lower. This may be due to lower air swirl velocity which is responsible for radial drop transport.

Figure 8 reports radial profiles of normalized mean drop size (d_{32}) obtained from the low flow numerical calculations at locations A, B, and C of figure 4, together with the corresponding experimental data. It can be observed that both the predictions and measurements exhibit the same qualitative trends at all three locations as observed in the high flow simulation. In contrast to figure 4, a sharp peak in the normalized SMD is observed from the CFD predictions near the centerline.

It is believed that this is due to a small number of intact (not atomized) large drops being entrained from the liquid stream into the inner air stream. This peak should be disregarded owing to the fact that the axial liquid volume flux at this location was extremely low. In fact, the PDA operating procedure for measuring drop sizes also suggests that drop size measurements should be disregarded where the particle number flux is low. It is believed that if the predictions had been post processed in a manner consistent with the PDA operating procedure, these peaks would not occur.

Figures 9a, b and c present plots of number *pdf* versus normalized drop size from the low flow simulations, together with corresponding experimental measurements, at

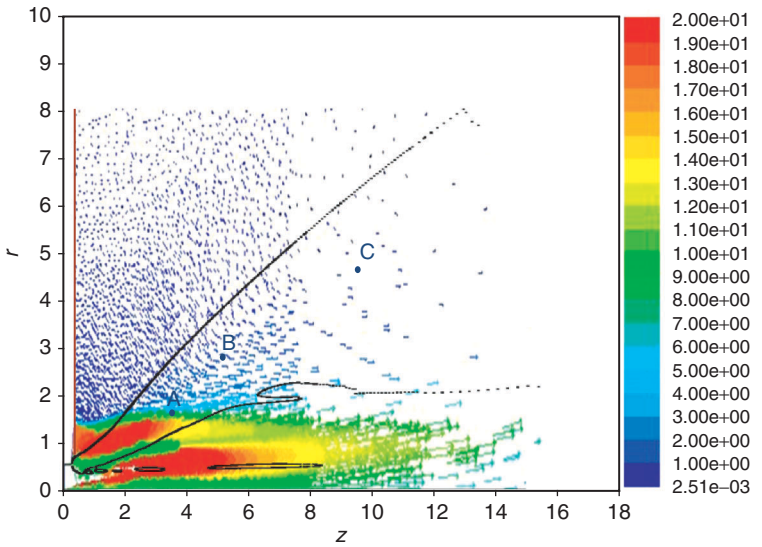

Figure 7: Spray profile (black dotted line) obtained from low flow condition simulation overlaid on a velocity vector plot colored by velocity magnitude (red and blue indicate highest and lowest velocities respectively).

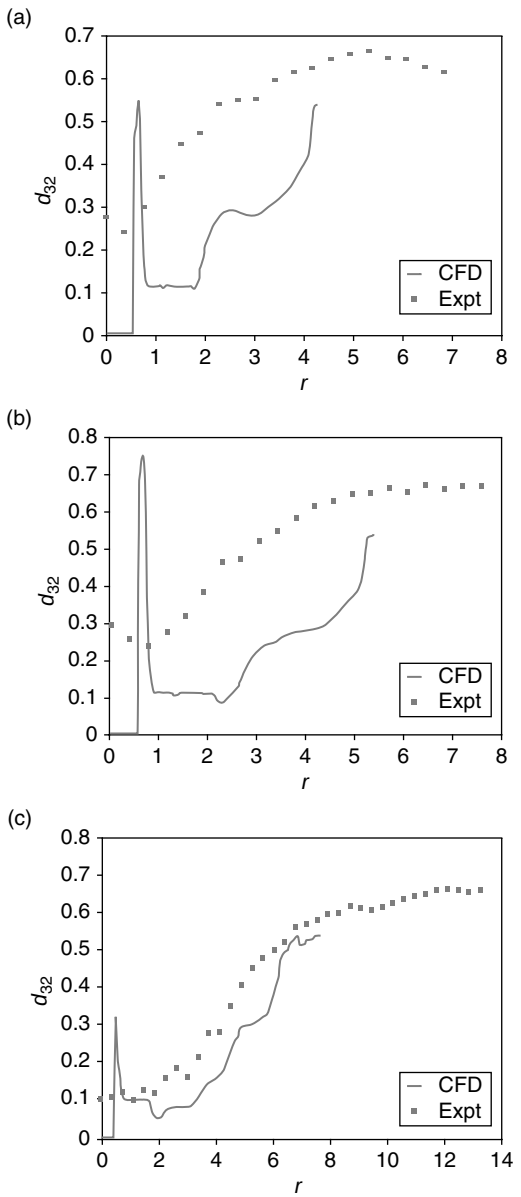

Figure 8: Radial profiles of normalized SMD obtained from the low flow condition simulation at axial locations of (a) 3.61, (b) 4.82 and (c) 9.84.

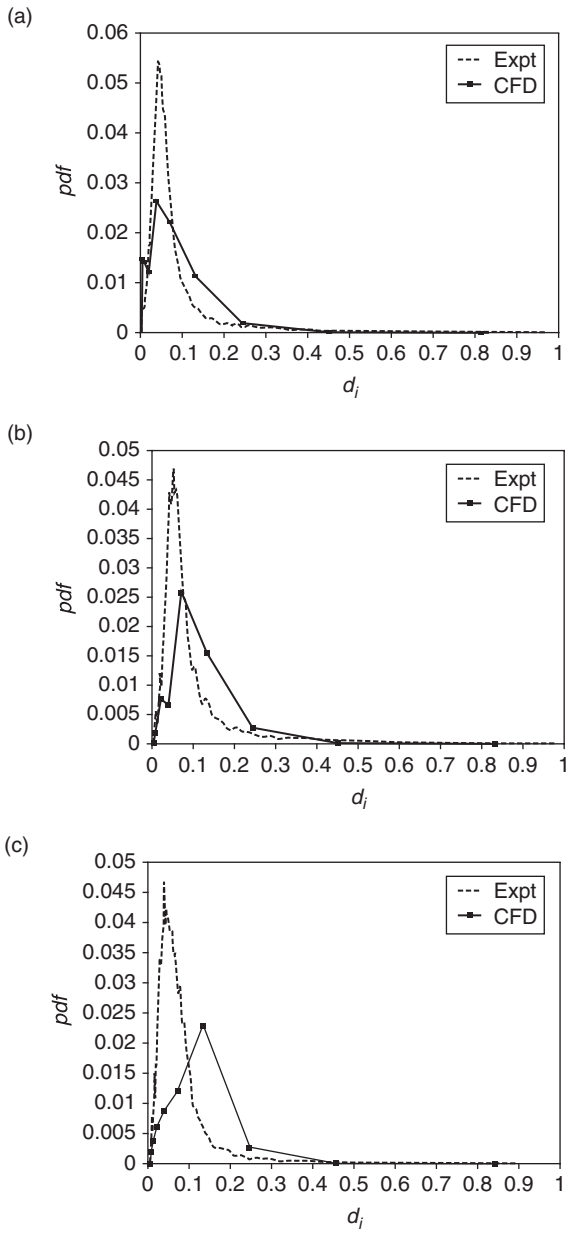

Figure 9: (a) Particle size distribution *pdf* at z = 3.61, r = 1.14 and at the low flow condition. (b) Particle size distribution *pdf* at z = 4.82, r = 2.66 and at the low flow condition. (c) Particle size distribution *pdf* at z = 9.64, r = 4.55 and at the low flow condition.

points A, B, and C of figure 7 where the liquid axial volume flux was sufficiently large and experimental data was available. While the agreement between measurements and predictions is acceptable in figures 9a and 9b, it is relatively poor in figure 9c.

Figure 10 plots predicted axial, radial and, swirl drop velocities versus drop size at point B of figure 9. In viewing this figure it is important to take into account the numerical artifact that the CFD model equates the velocity of a phase to zero when its volume fraction falls below a small critical value, which renders the reported zero velocities of the smallest three size classes unphysical. As mentioned previously, the full multiphase model employed herein allows each drop phase to exhibit an individual velocity (while, in contrast, mixture models require all drop phases to have a single velocity). It can be clearly observed from figure 10 that the drop velocities are predicted to be sensitive to drop size, thus indicating that a full multiphase model is required to accurately capture this behavior. It is believed that much of this velocity/size sensitivity is due to swirl, thus making the full multiphase approach especially appropriate for the simulation of swirling sprays. It would be interesting to determine whether an inhomogeneous multiple size group model, such as that discussed by Krepper et al. [31], could sufficiently capture the velocity/size sensitivity discussed above while reducing computational intensity. The full multiphase predictions presented herein should be valuable in answering this question.

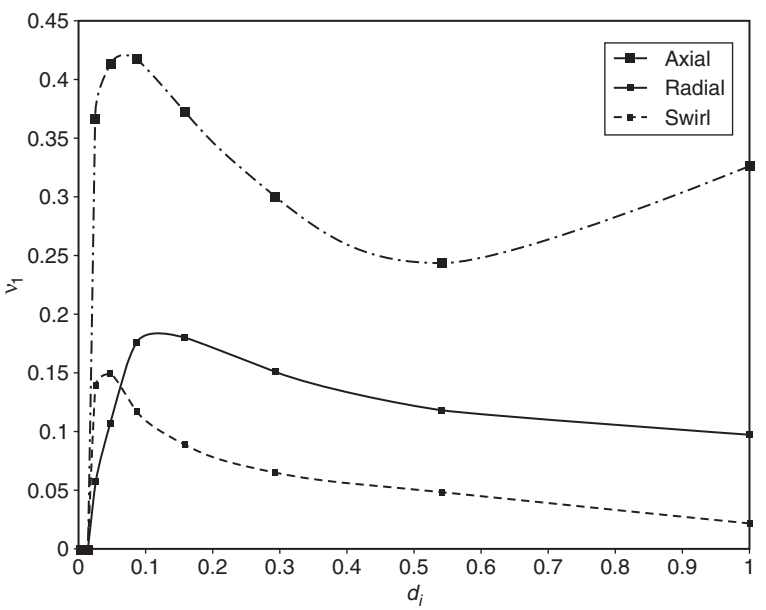

Figure 10: Particle phase velocity versus particle size at z = 4.82 and r = 2.26 for the high flow condition.

3.3. Discussion

The Eulerian multiphase model developed to study atomizing flows is observed to perform reasonably well in qualitatively predicting both SMD and point-wise particle size distributions, considering that the atomization model employs only two adjustable constants. In fact, it has been observed by Le Moyne [12] that this is the only feasible approach to predicting the spatial distribution of the drop size *pdf*. The model is also capable of capturing the qualitative phenomenon often observed in atomizing flows that the larger particles tend to be transported towards the outer periphery of the spray. The predictions contain qualitative inaccuracies but, in spite of these, it is believed that the method proposed herein can be used to compare results from geometry to geometry to infer trends in performance variation. Such a tool is valuable to design engineers in reducing design cycle times. The primary quantitative discrepancy between the PDPA data and the CFD predictions is in the volume flux results. While the former indicate non-zero spray volume fluxes on the centerline, the latter indicate near-zero spray volume fluxes there. This, in turn, produces lower predicted SMD values on the centerline than are indicated by the PDPA data. Part of this disagreement may be due to inaccurate PDPA data near the centerline (where the volume flux and the number data rate are small). In any case, the fact that the PDPA data for liquid volume fluxes do not satisfying mass continuity (a well known phenomenon) while the predicted liquid volume fluxes do makes it impossible to regard this quantitative disagreement as a defect of the model.

A number of potential causes can be postulated for the quantitative predictive inaccuracies mentioned above including (but not limited to) neglect of three-dimensional effects, neglect of drop phase diffusion, use of a single pressure model, the fact that FLUENT operates in such a way as to equate all variables associated with a given phase to zero at a location once the volume fraction of that phase has dropped below a small built in value at that location, and inability of the atomization model to capture the details of the process accurately. As mentioned earlier, the many remaining uncertainties in multiphase flow modeling make it extremely difficult to assign a specific disagreement between predictions and observations to a specific cause. This can be done only through a painstaking process of performing simulations with different models in such a way as to make modeling changes one at a time. While this is beyond the scope of the present paper, it is hoped that the present work can serve as a first step in such a process. A number of additional simulations were performed (see [27]) in order to test the sensitivity of predictions to the details of the atomization model. In no case was the qualitative nature of predictions found to be very sensitive to these details, so most are not discussed herein. One example is described in the next paragraph.

Figure 11 presents plots of the radial distribution of the d_{32} for $\Gamma_0 = 0.022$ (associated with the previous results) and $\Gamma_0 = 0.22$, in order to characterize the influence of Γ_0 on predictions.

While a 200–300% increase can be observed, these percentage increases are in small numbers and are the results of an order of magnitude increase in Γ_0. The inset shows a plot of the *pdf*'s for these two cases along with the corresponding experimental data at the point P in figure 11. It is clear from this inset figure that the peak in the drop size

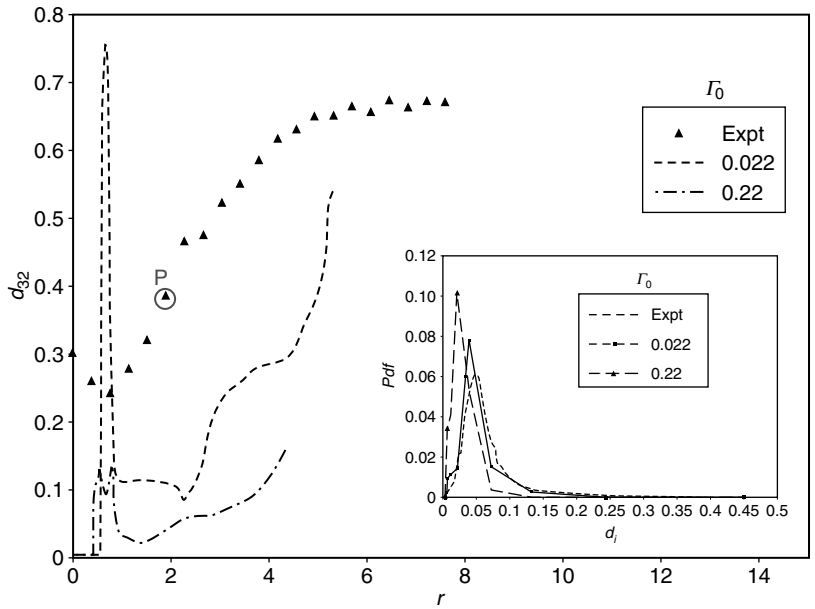

Figure 11: Radial profiles of normalized Sauter mean diameter obtained for different breakage frequency constants at z = 4.82. The inset figure shows the particle size distribution *pdf* at z = 4.82 and r = 1.9 (Point P).

distribution shifts towards smaller drop sizes indicating increased atomization with increasing Γ_0.

Several other comparisons between predictions and observations were made for additional nozzle configurations in the course of the work reported on herein (see [27]) These are not presented (for the sake of brevity) since the results already discussed were found to be qualitatively representative of all the configurations considered. The degree of qualitative agreement reported earlier between predictions and measurements suggests that these could be fruitfully used, in conjunction with the predictions presented herein, to carry out studies of the type mentioned earlier to evaluate the applicability of simpler models consistent with the fully multiphase model employed herein.

4. SUMMARY AND CONCLUSIONS

In this paper, the development of an Eulerian multiphase model for predicting the evolution of the particle size distribution in an atomization process is discussed. The Eulerian multiphase model is capable of handling atomization and transport processes simultaneously. This model incorporates M + 1 (M discrete + 1 continuous) phases, with each discrete phase representing one particle size class. As in any general multiphase model, each size class is allowed to have its own velocity field. The atomization is modeled as a cascade process which causes mass to be transferred between drop phases.

This was characterized using the discrete population balance approach and was implemented alongside FLUENT using user-defined mass and momentum source terms in the respective balance equations. This model was successfully validated against the analytical solution for the simple case of a uniform slug flow in a pipe problem. Numerical simulations were performed on different grid sizes to establish grid independence.

The model was then exercised for two sets of flow conditions where experimental data was available and the results compared. The following conclusions can be drawn from these results.

- An Eulerian multiphase model is needed to model the phasic velocity differences occurring in atomizing swirling fluid flow systems.
- The particle size distributions and their evolution were successfully predicted using the population balance approach.
- Model predictions compared favorably with experimental data in the test case of a swirling atomizing flow.
- To the best of our knowledge, this is the first effort at modeling atomization and transport in a multiphase framework.

REFERENCES

[1] R.O. Fox, F. Laurent and F. Massot, Numerical simulation of spray coalescence in an Eulerian framework: direct quadrature method of moments and multi-fluid model, *Journal of Computational Physics*, 2008, 277, 3058–3088.

[2] P. Chen, M.P. Dudukovic and J. Sanyal, Three dimesional simulation of bubble column flows with bubble coalescence and break up, *AIChE J.,* 2005, 51, 696–712.

[3] S. Ghaniyari-Benis, N. Hedayat, M. Ziyari, M. Kazemzadeh and M. Shafiee, Three-dimensional simulation of hydrodynamics in a rotating disk contactor using computational fluid dynamics, *Chemical Engineering Technology*, 2009, 32, 93–102.

[4] F. Kunz, M. Gibeling, G. Maxey, G. Tryggvason, A. Fontaine, H. Petrie and S. Ceccio, Validation of two-fluid Eulerian CFD modeling for microbubble drag reduction across a wide range of Reynolds numbers, *ASME Journal of Fluids Engineering*, 2007, 129, 66–79.

[5] A. Vallet, A.A. Burluka and R. Borghi, Development of a Eulerian model for the "Atomization" of a liquid jet, *Atomization and Sprays*, 2001, 11, 619–642.

[6] O. Sero-Guillame and N. Rimbert, On thermodynamic closures for two-phase flow with interfacial area concentration transport equation, *Int. J. Multiphase flow*, 2005, 31, 897–910.

[7] S. Jay, F. Lacas and S. Candel, Combined surface density concepts for dense spray combustion, *Combustion and Flame*, 2006, 144, 558–577.

[8] E. Deux and M. Sommerfeld, Modeling of turbulent atomization combining a two-fluid and a structure function approach, *Atomization and Sprays*, 2006, 16, 103–125.

[9] F.X. Demoulin, P.A. Beau, G. Blokkeel, A. Mura and R. Borghi, A new model for turbulent flows with large density fluctuations: Application to liquid atomization, *Atomization and Sprays*, 2007, 17, 315–345.

[10] F. Moukalled and M. Darwish, Mixing and evaporation of liquid droplets injected into an air stream flowing at all speeds, *Physics of Fluids*, 2008, 20, 040804.

[11] S.V. Apte, K. Mahesh and T. Lundgren, A Eulerian-Lagrangian model to simulate two-phase/particulate flows, in Annual Research Briefs, 2003, *Center for Turlbulence Research*: Palo Alto CA, 161–171.

[12] L. Le Moyne, Trends in atomization theory, *International Journal of Spray and Combustion Dynamics*, 2010, 2, 49–84.

[13] D. Ramkrishna, Population Balances, 2000, New York: *Academic Press*.

[14] FLUENT, FLUENT User Manual, 2008.

[15] B.E. Launder and D.B. Spalding, Lectures in Mathematical models of turbulence, 1972, London: *Academic press*.

[16] L. Schiller and Z. Naumann, A drag co-efficient correlation, *Z.Ver.Duetsch. Ing*., 1935, 77–318.

[17] A. Escue and J. Cui, Comparison of turbulence models in simulating swirling pipe flows, *Applied Mathematical Modelling*, 2010, 34, 2840–2849.

[18] M.A. Lopez de Bertodano and A.A. Saif, Modified k-ε model for two-phase turbulent jets, *Nuclear Engineering Design*, 1997, 172, 187–196.

[19] M. Lopez de Bertodano, Two fluid model for two-phase turbulent jet, *Nuclear Engineering and Design*, 1998, 179, 65–74.

[20] M. Lopez de Bertodano, M., F.J. Moraga, D.A. Drew and R.T. Lahey Jr., The Modeling of Lift and Dispersion Forces in Two-Fluid Model Simulations of a Bubbly Jet, *ASME Journal of Fluids Engineering*, 2004, 126, 573–577.

[21] R. You, J. Peddieson, J. Gadiyaram and S. Munukutla, Simulation of particle/fluid flows in vertical circular pipes, *International Journal of Non-linear Mechanics*, 2010, 455, 490–506.

[22] H.H. Qiu, W. Jia, C.T. Hsu and M. Sommerfeld, High accuracy optical particle sizing in phase-Doppler anemometry, *Measurement Science and Technology*, 2000, 11, 142–151.

[23] H. Koh and Y. Yoon. Spray measurement using optical line patternator, in *Liquid atomization and spray systems, ICLASS Conference*, 2005, Seoul, Korea.

[24] J.F. Widmann, C. Presser and S.D. Leigh, Improving phase Doppler volume flux measurements in low data rate applications, *Measurement Science and Technology*, 2001, 12, 1180–1190.

[25] S. Kumar and D. Ramkrishna, On the solution of population balance equations by discretization-I. A fixed pivot technique, *Chemical Engineering Science*, 1996, 51, 1311–1332.

[26] M. Gorokhovski and V.L. Saveliev, Analyses of Kolmogorov's model of breakup and it's application into Lagrangian computation of liquid sprays under air-blast atomization, *Phys. Fluids*, 2003, 15, 184–192.

[27] N.P. Rayapati, Eulerian multiphase model of fragmenting flows, in Mechanical Engineering, *PhD Thesis*, 2009, Tennessee Technological University: Cookeville TN.

[28] A.H. Lefebvre, Gas Turbine Combustion, 2nd ed. 1998: *Taylor & Francis*.

[29] K.J. Reid, A solution to the batch grinding equation, *Chemical Engineering Science*, 1965, 20, 953–963.

[30] S. Bhamidipati, M.V. Panchagnula, and J. Peddieson. Eulerian multi-fluid model of airblast atomization, in *ASME IMECE*. 2006, Chicago IL: ASME.

[31] E. Krepper, D. Lucas, T. Frank, H-M. Prasser and P.J. Zwart, The inhomogeneous MUSIG model for the simulation of polydispersed flows, *Nuclear Engineering and Design*, 2008, 238, 1690–1702.